Automated quantification of sewage pipe cracks using deep learning for urban water environment management

Yang, Chenhao ; Zheng, Feifei; Kapelan, Zoran; Savic, Dragan; Pan, Gang; Feng, Yu; Ma, Yiyi

DOI
10.1016/j.tust.2024.106195

Publication date
2024

Document Version
Final published version

Published in
Tunnelling and Underground Space Technology

Tunnelling and Underground Space Technology 155 (2025) 106195

Contents lists available at ScienceDirect

Tunnelling and Underground Space Technology incorporating Trenchless Technology Research

journal homepage: www.elsevier.com/locate/tust

Automated quantification of sewage pipe cracks using deep learning for urban water environment management

Chenhao Yang [a], Feifei Zheng [a], Zoran Kapelan [b,c], Dragan Savic [d,c,e], Gang Pan [f], Yu Feng [g], Yiyi Ma [a,*]

[a] College of Civil Engineering and Architecture, Zhejiang University, China
[b] Department of Water Management, Delft University of Technology, The Netherlands
[c] Centre for Water Systems, University of Exeter, North Park Road, Exeter EX4 4QF, United Kingdom
[d] KWR Water Research Institute, Netherlands
[e] Faculty of Civil Engineering, University of Belgrade, Serbia
[f] College of Intelligence and Computing, Tianjin University, China
[g] Chair of Cartography and Visual Analytics, Technical University of Munich, Germany

ARTICLE INFO

Keywords:
Automated quantification
CCTV
Deep learning
Pipe defect
Urban water environment management

ABSTRACT

Sewage pipe defects can significantly affect the urban water environment, like leakage of pollutants through pipe cracks to groundwater. Currently, sewage pipe defects are detected mainly through closed-circuit television inspection, which is conducted manually and is time-consuming. This study proposes an integrated deep-learning-based algorithm to detect and quantify pipe cracks from images, namely the Crack Detection and Characterization (CDC) method. The method is based on models created in two steps (i) crack detection by semantic segmentation, and (ii) crack length quantification using an innovative algorithm. The CDC algorithm is verified by images both artificially created in the laboratory and from actual inspection. For both laboratory and field cases, the CDC method is verified precisely. From the results, the CDC method exhibited a higher accuracy in crack identification and length quantification than other existing models. The results also show that the deblurring process can greatly improve accuracy. This study can contribute to decision-making in sewage pipe maintenance and water environment management by providing an innovative way of more efficient and accurate pipe defect assessment compared with traditional labor-intensive work.

1. Introduction

Urban sewage pipes are important urban infrastructures, which collect and transport industrial wastewater and domestic sewage for treatment and safe disposal. Because of pipe aging and inadequate maintenance, defects in sewage pipes, including deposits, cracks, root intrusion and infiltration, are increasingly severe (Okwori et al., 2021). These pipe defects can cause adverse environmental impacts like unexpected sewage leakage, water pollution, urban facility failure risks, etc. (Xu et al., 2019; Harpaz et al., 2022; Shi et al., 2023). Closed-circuit television (CCTV) is a typical underground sewage pipe inspection method. Currently, pipe defect detection from CCTV images is mostly conducted manually, which is time-consuming and labor-intensive. Also, due to the broad definition of pipe defect severity grades in the current standards, the pipe assessment results mainly depend on the inspectors' experience. Thus, manual interpretation of CCTV inspection images can usually be subjective and inaccurate (Sun et al., 2023). Considering the rapid development of pipe networks during urbanization processes, especially in developing countries, high-efficiency is urgently requested for maintenance and renewal of sewage pipes (Sun et al., 2023).

Lately, deep-learning-based algorithms have been proposed for automated detection of sewage pipe defects based on images extracted from CCTV videos to improve efficiency (Xie et al., 2019; Moradi et al., 2020; Haurum and Moeslund, 2020). Convolutional Neural Network (CNN) is one of the deep learning techniques. Plenty of CNN models have been developed to achieve the following: (1) object classification, which detects whether there are sewage pipe defects in CCTV images but

* Corresponding author.
E-mail addresses: 22212067@zju.edu.cn (C. Yang), feifeizheng@zju.edu.cn (F. Zheng), z.kapelan@tudelft.nl (Z. Kapelan), Dragan.Savic@kwrwater.nl (D. Savic), pangang@tju.edu.cn (G. Pan), y.feng@tum.de (Y. Feng), yiyima@zju.edu.cn (Y. Ma).

https://doi.org/10.1016/j.tust.2024.106195
Received 29 May 2024; Received in revised form 29 September 2024; Accepted 3 November 2024
Available online 19 November 2024

cannot locate the defects precisely (Kumar et al., 2018; Xie et al., 2019; Meijer et al., 2019; Hassan et al., 2019); (2) object localization, which can automatically detect, classify and locate pipe defects within the CCTV image (Wang et al., 2021; Guo et al., 2022; Wang et al., 2022); (3) semantic segmentation, which can identify/segment pipe defects at pixel-level (Pan et al., 2020; Li et al., 2022). However, object localization algorithms are commonly time-consuming to develop and use (Cheng and Wang, 2018; Oh et al., 2022; Wang et al., 2023; Yin et al., 2020; Zhao et al., 2023). In comparison, semantic segmentation can extract features of pipe defects more precisely (e.g., recognizing more details of the shape of defects) and can assist system inspectors in assessing the status of sewage pipes.

CNN-based algorithms, like fully convolutional networks (FCN), SegNet, U-Net, etc., have shown good performance in semantic segmentation (Pan et al., 2020; Ma et al., 2022), which can provide details of features such as the edge of cracks (He et al., 2022). However, it is difficult to make these methods accurate for simultaneous classification and segmentation. Even with proper segmentation of pipe images, assessing the severity of pipe defects manually is still labor-intensive. Automated characterization of sewage pipe defects (e.g., location, shape, orientation, and quantification of defects) is needed for more efficient pipe condition assessment.

Recently, 3D point cloud technology has been applied for automated characterization of sewage pipe defects (Li et al., 2023; Wang et al., 2024; Yin et al., 2022; Zhao et al., 2023). It can capture the geometry of objects and reconstruct the surface texture of objects, thus making it available for quantifying pipe defects. However, errors can be generated while constructing point cloud models due to the poor shooting environment inside pipes. Also, the model development requires many video data, which is usually not feasible. Automated characterization of pipe defects based on CCTV images can also be achieved by developing accurate segmentation algorithms along with characterization algorithms, although the number of relevant studies is small. Wang et al. (2021) and Guo et al. (2022) reported an area ratio calculating algorithm based on Faster R-CNN, which automatically quantified the severity of obstacles by scaling the obstacle size from the known pipe joint size. But its accuracy is affected dramatically by the distance between the obstacle and pipe joint, and does not perform well in some cases (Wang et al., 2021; Jia et al., 2023). Even so, it provides an innovative method for the automated characterization of sewage pipe defects based on CCTV images.

Summarized from the literature review, the major problems in the detection and characterization of sewage defects from CCTV images using deep-learning-based technologies include (1) inadequate accuracy of detection due to the complex environment inside sewage pipes, (2) slow computation speed due to extensive cost of computational resources, and (3) a lack of accurate quantification methods for pipe defects.

Cracks are one of the most frequently observed defects in urban sewage pipes. They can cause adverse environmental impacts through exfiltration of sewage, which leads to urban water environment pollution and thus threats human health (Baah et al., 2015; Wang et al., 2023). This study aims to address the problem of automated quantification of sewage pipe defects, taking cracks as an example, to provide an efficient and accurate method for pipe condition evaluation. To address the above the accuracy and cost problem occurring to the area ratio calculating methods and 3D reconstruction, an integrated algorithm is developed in this study, which consists of both pipe crack detection and innovative characterization models. The main aim is to demonstrate that the new algorithm can improve accuracy over the existing approaches, accelerate the computation processes, achieve better transfer learning, and reduce the need for manual interventions.

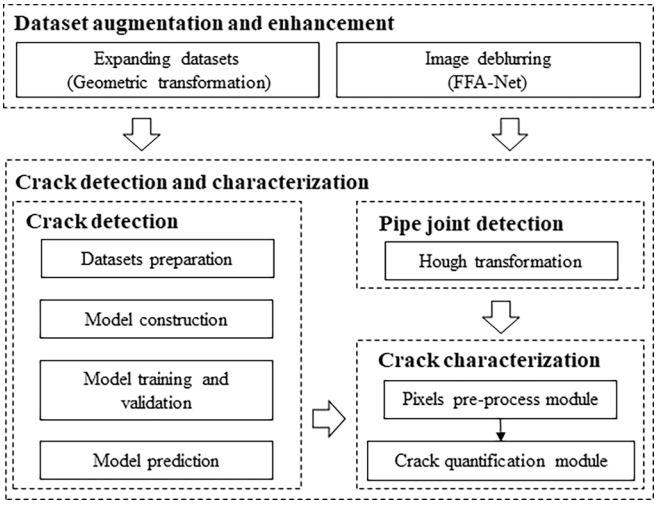

Fig. 1. Proposed algorithm for automated quantification of sewage pipe cracks.

2. Methodology

2.1. Architecture of the proposed method

The integrated algorithm proposed in this study is named the Crack Detection and Characterization (CDC) method. The algorithm combines computer vision techniques and innovative characterization algorithms, as illustrated in Fig. 1. The overall workflow of the integrated algorithm includes the following steps: (1) dataset augmentation and enhancement, i.e., using the geometric transformation and a deblurring algorithm for dataset expansion and CCTV image pre-processing; (2) crack detection from images via semantic segmentation; (3) pipe joint detection, i.e., identifying the center of the pipe cross-section and establishing the coordinate in CCTV images; and (4) crack characterization, i.e., quantifying the crack length. The details of the proposed algorithms are introduced in the following sections.

2.1.1. Datasets augmentation and enhancement

Since the internal environment of sewage pipes is usually causing blurry images, deblurring is required (Li et al., 2022; Ma et al., 2022). FFANet (Qin et al., 2020) is the deblurring algorithm applied in this study to improve the image quality. Additionally, the training of deep learning algorithms needs a large number of annotated images, while available data is often limited. It is, therefore, helpful to expand the existing dataset to obtain more available images for training (Altabey et al., 2021). In this study, to expand the datasets, geometric transformation of CCTV images is conducted, such as rotation, width shift, height shift, shear and zoom. The maximum rotation angle is set to 40°, and the range of shift, shear and zoom are set to 0.1, 0.2, 0.2 times the original image size. The datasets are then randomly divided into the training subset, the validation subset, and the test subset. The specific groupings for different cases are illustrated in the subsequent sections.

2.1.2. Crack detection

In this study, we use DeepLab V3 + detection model (i.e., segmentation model) to locate pipe cracks within the CCTV images (Chen et al., 2018). DeepLab V3 + is designed in Encoder-Decoder mode, as shown in Fig. 2**(a)**. Encoder outputs low-level features (i.e., overall shape features of pipe cracks) and high-level features (i.e., detailed edge features of pipe cracks). Decoder is used to recover the crack feature image. The backbone is the main structure of DeepLab V3 + for extracting features from images. Different structures of the backbone can lead to various results of semantic segmentation. In this study, two classical types of backbones, namely, Xception-65 and MobileNet V2, are tested and their performance in semantic segmentation is compared. The image features

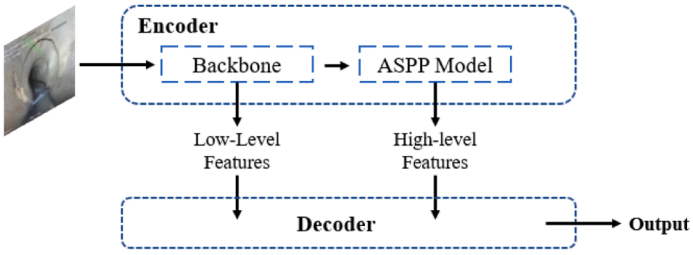

(a)

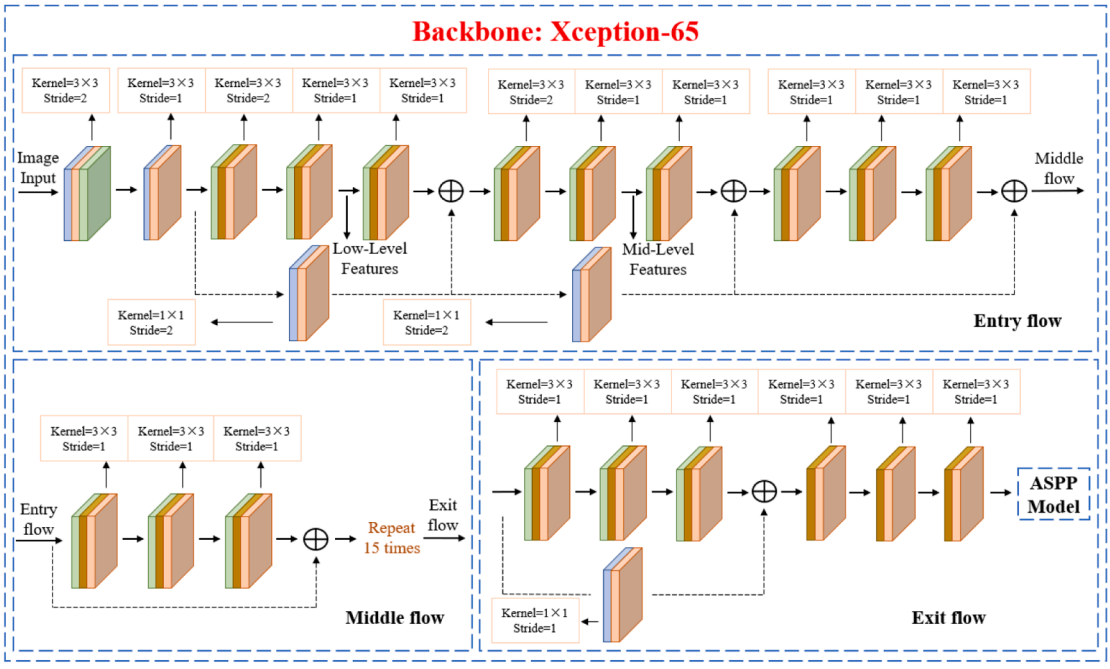

(b)

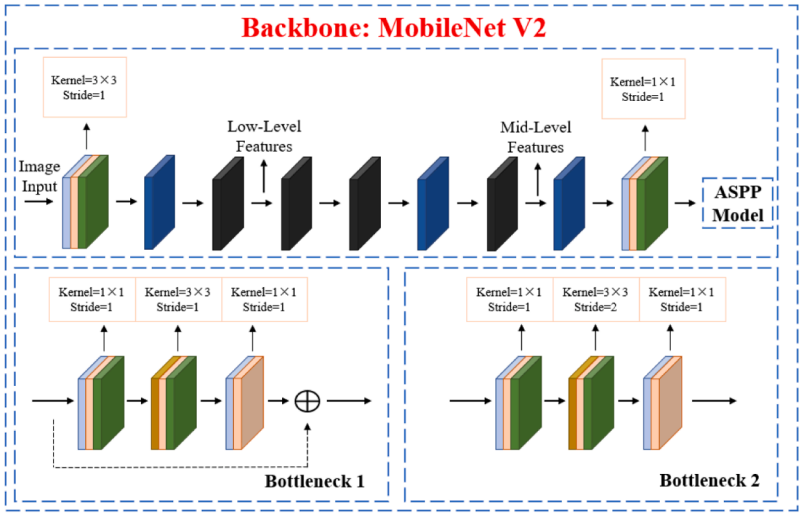

(c)

Fig. 2. Architecture of DeepLab V3+: (a) Encoder-Decoder mode; (b) backbone Xception-65; (c) backbone MobileNet V2; (d) ASPP; (e) decoder.

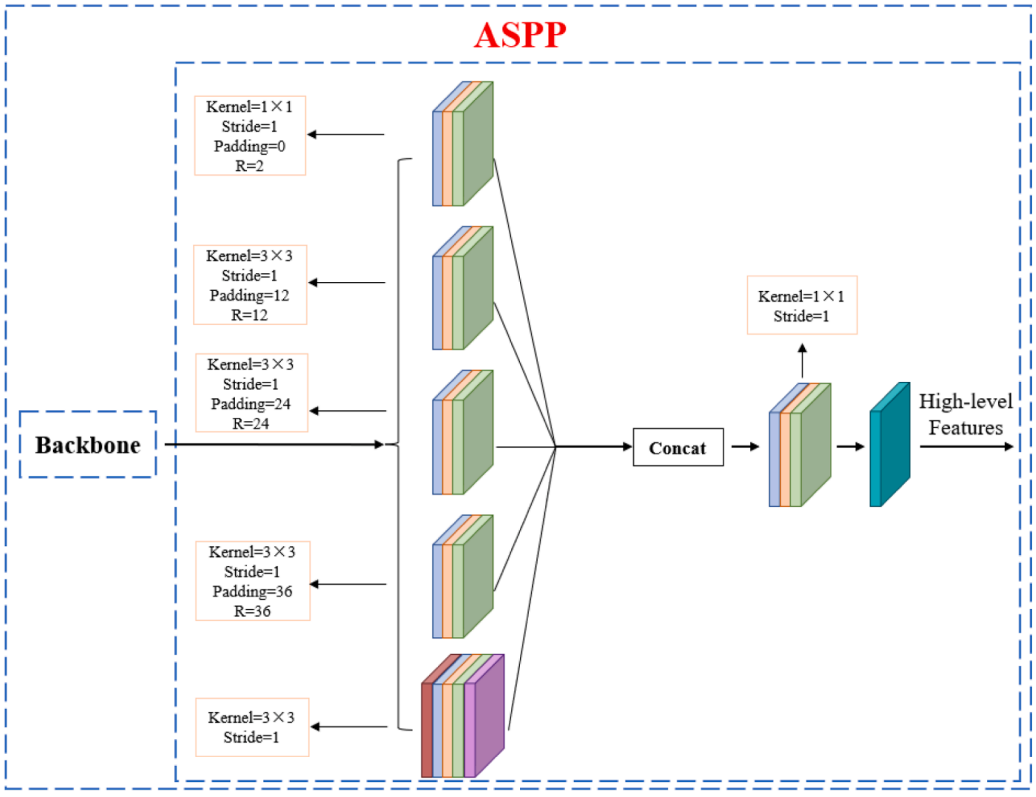

(d)

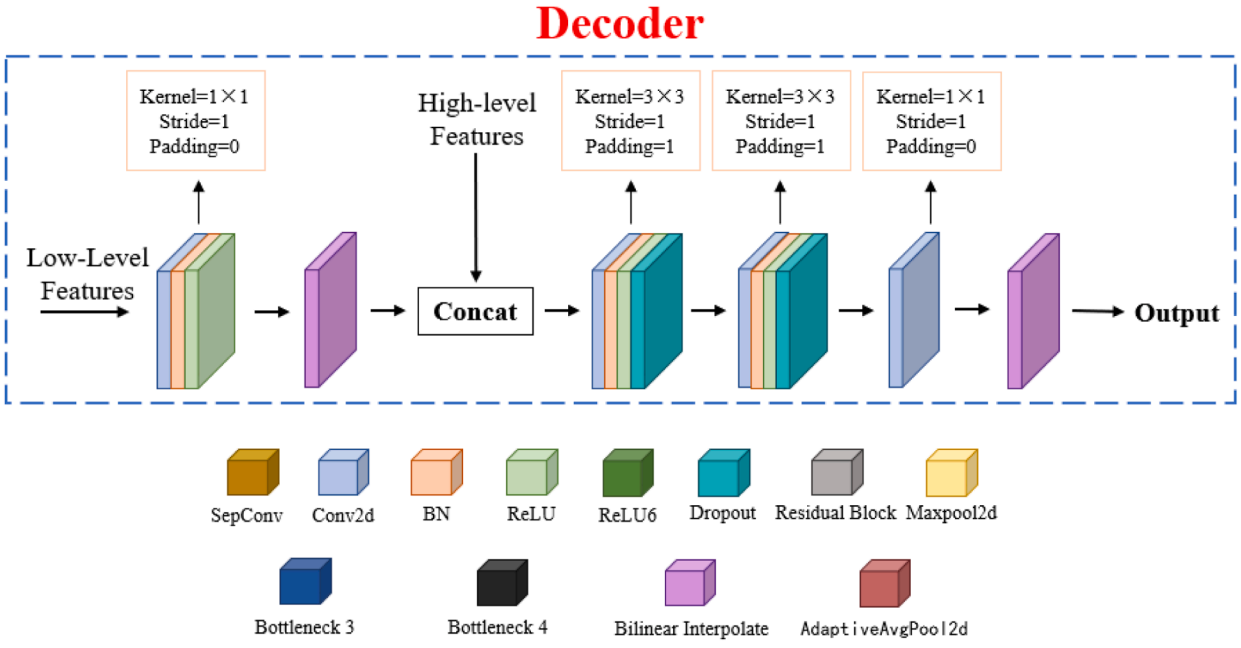

(e)

Fig. 2. (*continued*).

extracted from the backbone structure are then passed to ASPP architecture for further processing, which connects all the convolution operations in parallel and then concatenates them in the Concat layer (i.e., combines different information of crack features from different perspectives). Details of the backbone, ASPP, decoder, and other main parameters used in the proposed algorithm are introduced below.

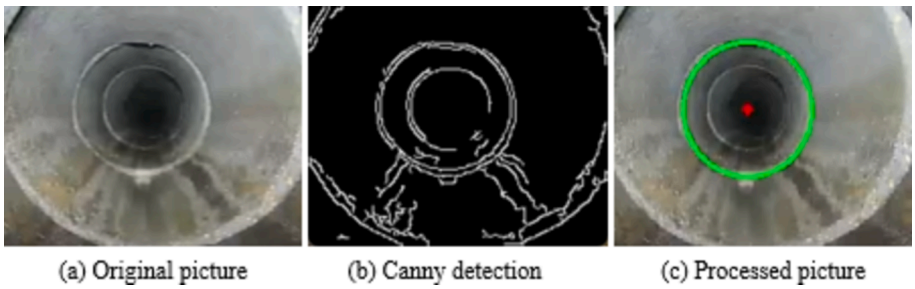

Fig. 3. Example of pipe joint detection using Hough transformation.

2.1.2.1. Backbone: Xception-65. As shown in Fig. 2**(b)**, there are three main parts in Xception-65, including Entry flow, Middle flow and Exit flow. In Entry flow, the CCTV image passes two common convolution layers first. Then, the crack features are extracted preliminarily by three residual connection structures to initiate the network of the algorithm. In the Middle flow, a large number of crack features are extracted and integrated. In Exit flow, the low-level and high-level features are transmitted from Decoder structure and ASPP architecture. The Xception-65 with its complex architecture can extract more complicated crack features, and thus, a more realistic crack segmentation image can be obtained.

2.1.2.2. Backbone: MobileNet V2. As shown in Fig. 2**(c)**, MobileNet V2 utilizes an inverted residual block for a better feature fusion of cracks (i.e., integrating the information from nearby layers), and makes the algorithm efficient for processing complex cracks. Meanwhile, ReLU6 is used as an activation function which can be calculated as follows:

$$y = \min(\max(x, 0), 6) \tag{1}$$

In ReLU6, the maximum output value is limited to 6, alleviating the accuracy degradation problem in training (Ravanbakhsh et al., 2016). It also solves the problem of activation function failure caused by the highly inaccurate segmentation to cracks when many complex structures are used at the same time. Because of the more straightforward structure, MobileNet V2 calculations are fast but less precise than Xception-65.

2.1.2.3. ASPP. As shown in Fig. 2**(d)**, DeepLab V3 + applies the ASPP to extract features further. The ASPP consists of the average pooling layer, convolutional layer, batch normalization (BN) layer, ReLU layer and bilinear interpolation. It performs better and can obtain more details of crack features (e.g., crack edge details) than other CNN-based models, like FCN and U-Net. Meanwhile, different dilated rates are set to each branch in ASPP, making the algorithm capable of extracting different features from various receptive-field sizes.

2.1.2.4. Decoder. In the Encoder structure, as shown in Fig. 2(e), low-level and high-level features are transmitted to the Decoder structure from the backbone and ASPP architecture, respectively. Then, they are integrated to re-construct the pipe crack.

2.1.3. Pipe joint detection

In this study, Hough transformation (Duda and Hart, 1972) is utilized to detect the pipe joint and get the center coordinates of the pipe cross-section from images. Fig. 3 shows an example of pipe joint detection by the Hough transformation. Specifically, before the transformation, the Canny edge detection (Canny, 1986) is used to extract the edges from the pipe photo (a group of points shown in Fig. 3b). Then, three points on the identified edges were randomly selected by applying Hough transformation, and a circle could be fitted using these three points. After repeating such fitting processes, many circles could be obtained. Among them, the one passing through the maximum points is considered as the detected pipe joint. That is then used as the length scale for the subsequent crack characterization considering the known diameter. It should be mentioned that although the least square algorithm is also capable of pipe joints detection (Wang et al., 2021), for discontinuous edge

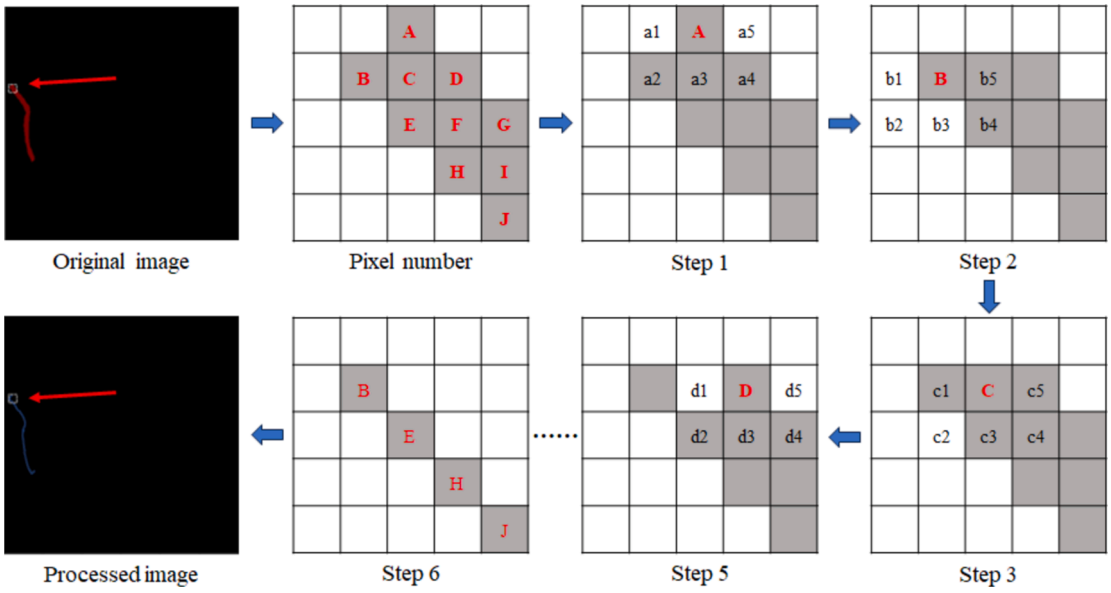

Fig. 4. Processing crack to unit width.

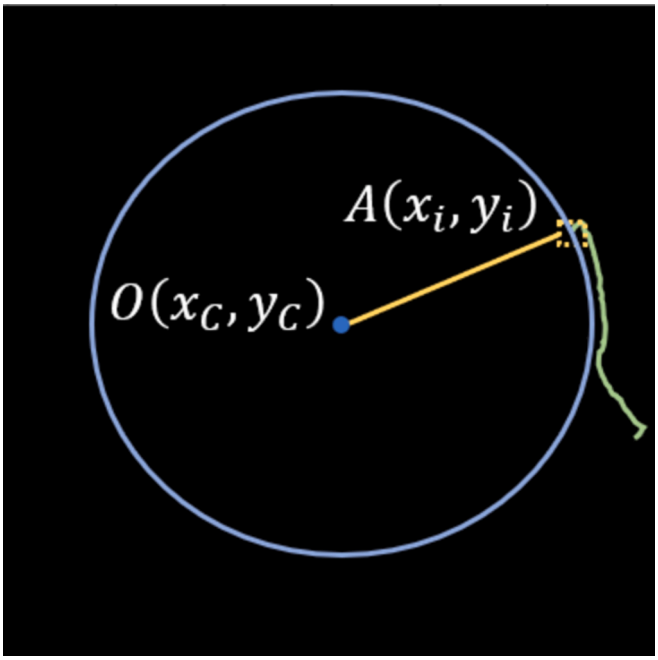

Fig. 5. Principle of crack characterization.

scenarios, like the current case shown in Fig. 3b, Hough transformation is more accurate and more robust to noise.

2.1.4. Crack characterization

The crack characterization algorithm is developed to quantify the pipe crack length from CCTV images, as illustrated in Fig. 1. It consists of two steps involving crack pixel processing and characterization, respectively. The crack shown in Fig. 4 is taken as an example. The image is black and white, so the values of the pixels on the crack are 1 (e.g., pixels A-J in Fig. 4) while the others are 0. Scan the pixels on the crack from left to right. For a specific pixel, if there are at least three non-zero pixels concavely surrounding it, the value of this pixel is manually set to 0, as the pixel A in step 1 (a2, a3 and a4 among a1-a5 are non-zero pixels). In step 2, since only two non-zero pixels concavely surround the pixel B (i.e., b4 and b5), its value keeps 1. In step 3, there are four non-zero pixels (i.e., c1, c3, c4, and c5), the value of the pixel C is set to 0. Similarly, in step 4, three non-zero pixels are around the pixel D, and it is assigned to 0. After processing all the pixels on the crack in sequence, the crack width is finally reduced to one pixel (i.e., unit width), as shown in step 6 in Fig. 4. Then, the crack length can be obtained as the number of the remaining pixels.

Once the coordinates of the pipe joint center $O(x_c, y_c)$ are determined with the Hough circle detection algorithm, the crack length is then quantified using the following procedure. As shown in Fig. 5, considering the pixel $A(x_i, y_i)$ on the crack, a new circle is drawn with the center is O and the radius is the distance between A and O. Then the perimeters of the circle C_i (unit: pixel) and that of the actual drainage pipe C_s (unit: mm) are calculated as:

$$\begin{cases} C_i = 2\pi\sqrt{(y_i - y_c)^2 + (x_i - x_c)^2} \\ C_s = 2\pi R_s \end{cases} \tag{2}$$

where R_s (unit: mm) is the real inner radius of the sewage pipe and is known. The actual length of each pixel on this circle representing (i.e., the length scale) is calculated as follows:

$$\lambda_i = \frac{C_s}{C_i} = \frac{R_s}{\sqrt{(y_i - y_c)^2 + (x_i - x_c)^2}} \tag{3}$$

where,λ_i is the length scale, mm/pixel. The actual length of the pixel A representing is then calculated. By repeating calculating the actual length of every pixel on the crack (L_i), the crack length then can be obtained as follows:

$$L = \alpha \sum_{i=1}^{N} L_i \tag{4}$$

where N is the total amount of pixels on the crack in the segmentation image. Since the image resolution can bring some uncertainties in crack length quantification, a correction factor α is introduced in **Eq. (4)**. The value of α is determined by the quality of crack images. In this study, the correction factor will be tested preliminarily in the experiment. It is noted that the crack characterization algorithm proposed in this study is realized by scaling each pixel in the image to the actual length. Since the "pixel" is the minimum unit of the image, the width, height, and diagonal size of a single pixel are considered the same.

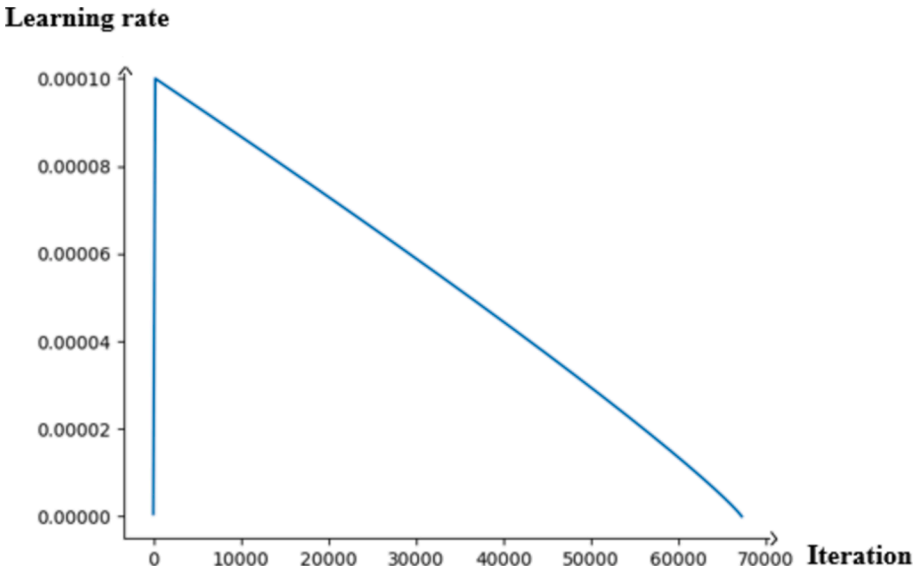

Fig. 6. Learning Rate Policy in the training process of DeepLab V3+.

2.2. Training and validation of crack detection model

The loss in training and validation is an indicator of the error in training a model. The loss calculation is based on the Cross-Entropy loss function, as follows:

$$L = -[y\log y' + (1-y)\log(1-y')] \tag{6}$$

where y is the real label value in images ($y = 1$ for true value and 0 for false value), and $y' \in (0, 1)$ is the predicted probability (e.g., if $y' = 0.8$, there is a possibility of 80 % that the value of the crack pixel is correct). Applying the Cross-Entropy loss function can prevent gradient dispersion and abnormal changes in learning rate. Additionally, in DeepLab V3+, the crop size is set to 520 × 520, which can improve the crack segmentation accuracy significantly.

The Learning Rate Policy is introduced when setting the learning rate for the DeepLab V3 + model. Validated by Pascal VOC 2012 dataset (Everingham et al., 2010), the Learning Rate Policy can improve the accuracy. The equation for Learning Rate Policy is as follows:

$$Lr = Lr \times \left(1 - \frac{Step}{Total\_Step}\right) \times Power \tag{7}$$

where *Power* is the learning rate correction factor (*Power* = 0.9 is used in this study for a stable training process). The learning rate is upgraded at every step. In addition, the warm-up method (He et al., 2016) is utilized in determining the learning rate. As shown in Fig. 6, with the warm-up method, the learning rate increases sharply from 0 to the pre-set value and then decreases gradually. This approach can alleviate the overfitting phenomenon and stabilize the algorithm for better segmentation in crack detection.

Crack detection models were trained and validated on a Windows system with 12th Gen Intel® Core™ i7-12700KF (20 CPUs) and NVIDIA GeForce RTX 3080 with 10G memory. Considering the image resolutions, the batch size was set to 2 after various tests, which made the most of the GPU (8.8G). For the model optimizer, SGD and Adam (Diederik and Jimmy, 2014) are both widely used. In this study, Adam with an initial learning rate of 0.0001 was utilized for the model. It can automatically adjust the learning rate during training, which is more efficient than SGD optimizer, especially for the training of complex models and datasets (Pan et al. 2020, Xie et al. 2019, Dang et al. 2021, and Oh et al. 2022). With the Learning Rate Policy and the warm-up method, Adam optimizer can further improve the training efficiency.

2.3. Performance evaluation method

2.3.1. Evaluation method for crack detection models

Intersection over union (IoU) and mean intersection over union (mIoU) are indexes for evaluating the effectiveness of models (Wang and Cheng, 2019; Pan et al., 2020), which are calculated based on a confusion matrix. In the confusion matrix, four parameters present the relationship between real values and predicted values, including True Positive (TP), False Negative (FN), False Positive (FP), and True Negative (TN). Both FN (i.e., a pixel outside the crack zone is recognized as a part of the crack) and FP (i.e., a pixel on the crack is not recognized) represent false predictions, while TP and TN represent the correct prediction. IoU represents the similarity between predicted results and true values, calculated as **Eq. (8)**:

$$IoU_i = \frac{TP_i}{TP_i + FN_i + FP_i} \tag{8}$$

mIoU indicates the mean IoU of each category, which is calculated as **Eq. (9)**:

$$mIoU = \frac{\sum_{i=1}^{n} IoU_i}{n} (i = 1, 2, \cdots, n) \tag{9}$$

Table 1
Specifications of urban drainage pipe crack grade*.

Grade	Definition	Sample image
1	Crack length is less than one-quarter of a pipe section.	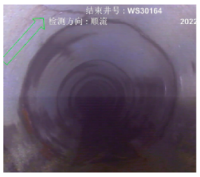
2	Crack length is one-quarter to two-quarters of a pipe section.	
3	Crack length is two-quarters to three-quarters of a pipe section.	
4	Crack length is more than three-quarters of a pipe section.	

* The table is based on Technical Specification for Inspection and Evaluation of Urban Drainage CJJ 181–2012 (National Development and Reform Commission of the People's Republic of China, 2012).

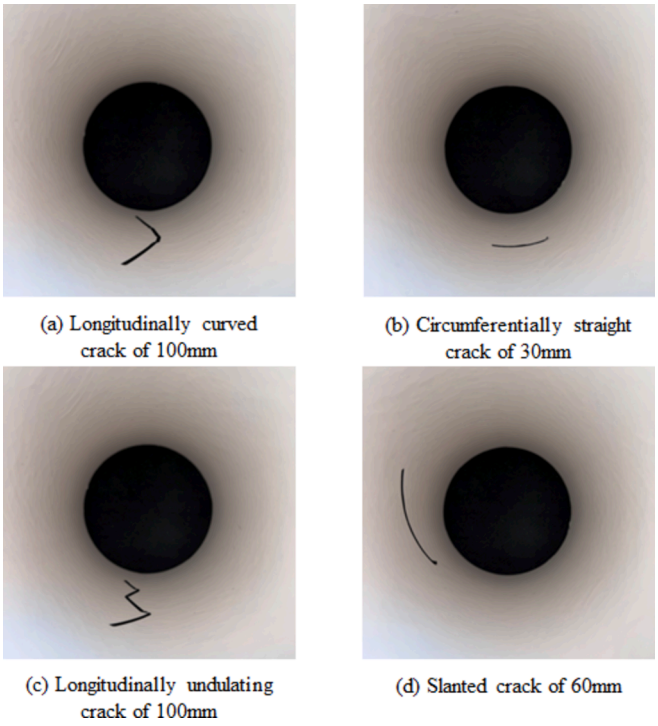

Fig. 7. Artificially-created cracks of different forms and lengths.

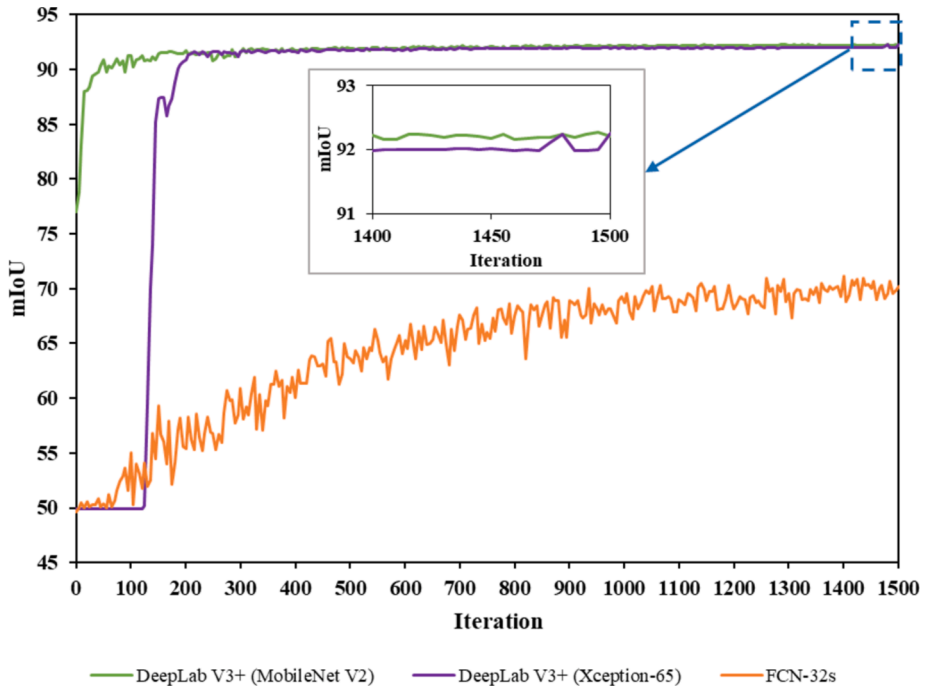

Fig. 8. Variation of mIoUs of three models during the training process.

A higher value of IoU or mIoU means a higher model accuracy.

2.3.2. *Evaluation method for crack characterization algorithm*

It is challenging to measure the lengths of cracks directly from actual sewage pipes. Grades of pipe crack lengths are usually identified from CCTV images manually and recorded in the field reports. In China, the pipe crack length is graded based on *Technical Specification for Inspection and Evaluation of Urban Drainage CJJ 181–2012* (National Development and Reform Commission of the People's Republic of China, 2012), according to the crack length estimated from CCTV inspection images, as shown in Table 1. In this study, the crack length results calculated by the proposed algorithm from actual CCTV images are validated against the field inspection reports where crack grades are provided according to the above technical specifications.

3. Results and discussion

In this section, we verify the performance of the proposed CDC algorithm with both laboratory cases and field cases, where the pipe cracks are artificially created and from real CCTV inspection projects, respectively. In the laboratory cases, the forms of cracks are controllable, and their lengths are known precisely. The laboratory cases are

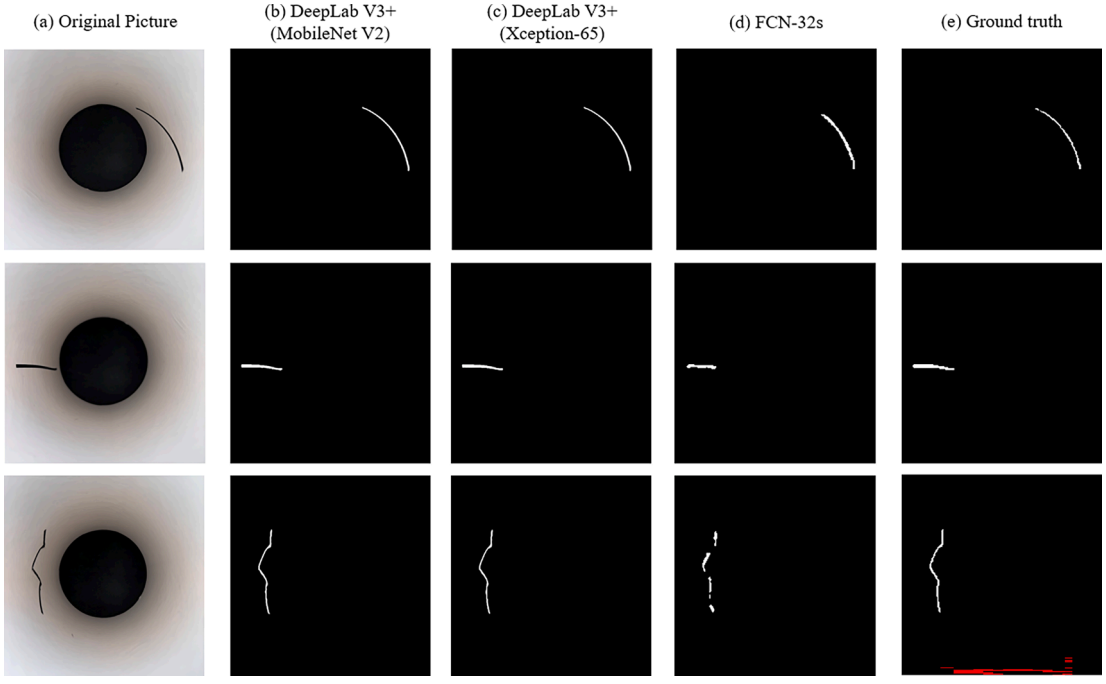

Fig. 9. Semantic segmentation results of the three models.

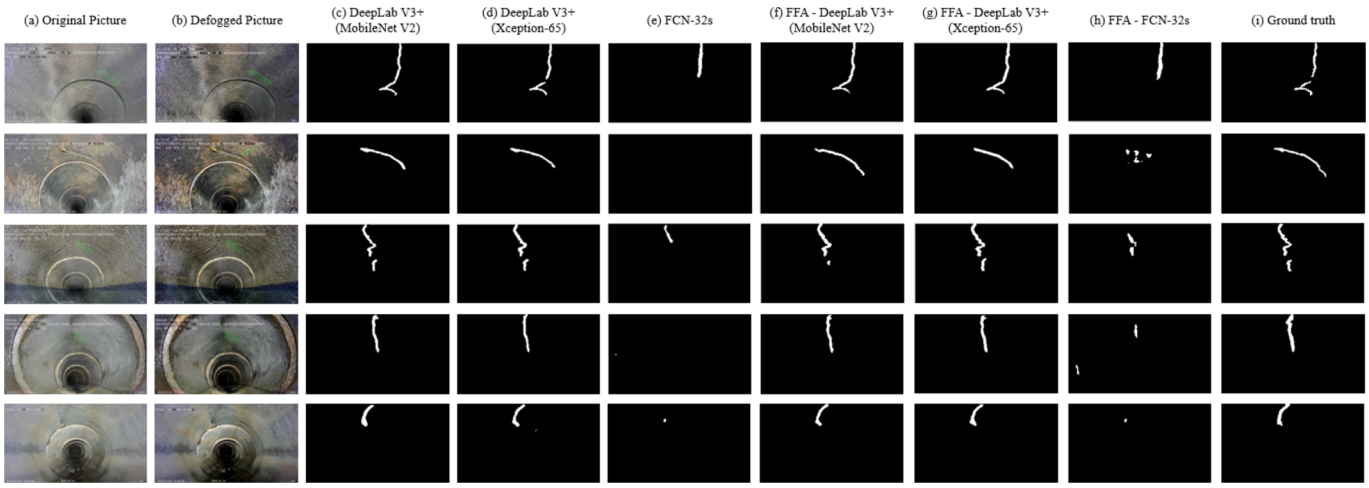

Fig. 10. Results of the semantic segmentation model.

used to verify the accuracy of the CDC algorithm with known crack lengths precisely, which has not been conducted by previous studies. The pipe crack images of the field cases (with lower resolution and usually foggy conditions) are used to test the performance of the CDC algorithm in real scenarios.

3.1. Laboratory cases

3.1.1. Dataset preparation

To verify the performance of the proposed algorithm, cracks in various directions and of different lengths were artificially created in a 100-mm-diameter PVC pipe in the laboratory, and their photos were recorded, as shown in Fig. 7. When taking photos, the camera was aligned with the longitudinal central axis of the pipe. The images were taken at a resolution of 3024 × 3024 pixels, and there is no blur in the view under the laboratory condition. The images obtained from the laboratory experiments are high-quality; thus, the number of images used for model training can be reduced. In this study, a total of 100 such images were utilized to train the segmentation model, of which 70 images were used for training and 30 for validation. With the geometric transformation of the images, the training data were augmented to 350. The images were annotated using a graphical image annotation tool Labelme, which exports documents for establishing datasets containing the information on background and cracks (Torralba et al., 2010).

3.1.2. Evaluation of crack detection models

Two DeepLab V3 + segmentation models with MobileNet V2 and Xception-65 backbones were tested to optimize the crack detection algorithm. The FCN-32 s model with ResNet101 backbone was trained to compare with the performance of DeepLab V3 + . Eventually, the three models were trained for 1,500 iterations, sufficient for stabilizing the training process based on loss calculation and mIoU development, as shown in Fig. 8. The training process took 40 h of computational time for each model. The semantic segmentation results are shown in Fig. 9.

Fig. 8 shows that the curves corresponding to mIoUs of DeepLab V3 + models are located above that of FCN-32 s model, indicating a more accurate crack detection by DeepLab V3 + models. Also, the two DeepLab V3 + models with MobileNet V2 and Xception-65 backbones have similar segmentation accuracies. However, the training of DeepLab V3+ (Xception-65) tends to overfit, as shown in Fig. 8 (enlarged section of the figure), indicating poorer stability than DeepLab V3+ (MobileNet V2) model in the first 500 iterations.

As seen from Fig. 9, the cracks segmented by the FCN-32 s model are incomplete compared to those segmented by the DeepLab V3 + models and ground truth images (cracks outlined manually from images).

3.1.3. Evaluation of crack characterization algorithm

The performance of the CDC algorithm in pipe crack characterization is first tested with various forms of artificially created cracks along different directions, including curved cracks, undulating cracks, and oblique cracks (Fig. 10). The lengths of these cracks were set to be 30 mm, 60 mm and 100 mm in the laboratory, which are typical lengths of three different crack grades identified in Technical Specification for Inspection and Evaluation of Urban Drainage CJJ 181–2012 (National Development and Reform Commission of the People's Republic of China, 2012). Images taken from four different perspectives were selected for each specific crack, and the averaged value calculated from the four images was used for model validation. Under the laboratory condition, images were captured with a resolution of 3024 × 3024 pixels. To measure the accuracy of the proposed algorithm for crack

Table 2
Crack characterization results by various models (unit: mm).

Crack lengths	30 mm			60 mm			100 mm		
Crack forms	DL (M) *	DL (X) *	FCN*	DL (M)	DL (X)	FCN	DL (M)	DL (X)	FCN
Vertically straight crack	25.17	25.45	17.00	49.09	66.55	33.00	71.72	75.04	58.00
Vertically curved crack	36.26	36.38	21.00	46.38	46.14	36.00	93.09	91.48	64.00
Vertically undulating crack	28.17	28.49	24.00	65.17	67.14	38.00	102.62	99.93	57.00
Slanted crack	37.67	38.15	24.00	79.86	74.11	45.00	129.30	129.46	82.00
Horizontally straight crack	37.79	32.76	39.00	79.55	84.74	52.00	129.06	131.33	115.00
Horizontally curved crack	37.62	37.80	41.00	77.44	78.81	68.00	127.47	125.14	137.00
Horizontally undulating crack	36.76	35.92	36.00	73.57	74.60	53.00	127.66	126.47	83.00
MSE	**41.30**	**33.37**	**80.00**	**228.08**	**237.76**	**313.00**	**582.40**	**553.96**	**1016.57**

* DL (M) = CDC algorithm combined with DeepLab V3 + (MobileNet V2); DL (X) = CDC algorithm combined with DeepLab V3 + (Xception-65); FCN = CDC algorithm combined with FCN-32 s.

Table 3
Dataset of the field cases.

	Guangzhou	Hangzhou	Sewer-ML	Total
Training	350	115	445	910
Validation	30	10	60	100
Total	380	125	505	1010

length quantification, mean squared error (MSE) is used, which is calculated as follows:

$$MSE = \frac{1}{N}\sum_{i=1}^{N}(observed_i - predicted_i)^2 \quad (10)$$

where N is the total number of all the cracks of the same length but different morphologies, $observed_i$ and $predicted_i$ are the actual and calculated crack lengths, respectively.

The MSEs of the CDC algorithm, combined with different crack detection models, for different pipe cracks are listed in Table 2. The results indicate that the CDC algorithm based on the DeepLab V3 + model has a higher accuracy (i.e., lower MSE values) under all the conditions than the model combined with the FCN-32 s algorithm. Also, for the CDC algorithm based on the DeepLab V3 + models of MobileNet V2 and Xception-65 backbones, the values of MSEs are similar. This is because the accuracy of crack length quantification depends significantly on the segmentation accuracy. It also needs to be noted that the crack characterization accuracy of the proposed CDC algorithm for longitudinal cracks (Fig. 7**a**) was lower than that for circumferential cracks (Fig. 7**b**). Such uncertainties are mainly caused by the limitation of CCTV cameras. When the end of the longitudinal crack is far from the camera focal plane, it appears blurred in the image. But the uncertainties are still under control. The results in Table 2 show that the maximum deviation between the prediction and the actual crack length is less than 30 %. This is because, in the length quantification algorithm, each pixel in the crack segmentation images was scaled to its actual length based on the pipe joints. Most of the longitudinal cracks can be captured clearly, and the blurry part occupies only a tiny portion of the total length.

To further verify the applicability of the proposed CDC algorithm in practice, its performance is checked with actual CCTV images, of which the image resolution is much lower and with more noise present in the view. It will be discussed in Section 3.2.

3.2. Field validation

3.2.1. Dataset preparation

The actual CCTV inspection images of sewage pipes in Guangzhou and Hangzhou, China, were used to further verify the performance of the CDC algorithm. Additionally, CCTV images from the Sewer-ML dataset (Haurum and Moeslund, 2021) were used for model training, too. The 282 images, of which 100 were from Guangzhou, 33 from Hangzhou and 149 from Sewer-ML, were mixed and divided into training and validation datasets. A total of 182 images (70 from Guangzhou, 23 from Hangzhou and 89 from Sewer-ML) were used for training, while 100 images (30 from Guangzhou, 10 from Hangzhou and 60 from Sewer-ML) were used for validation. As shown in Table 3, using the geometric transformation method introduced in Section 3.1.1, the training data was expanded to 1,010 images. Due to the blur in the actual CCTV images, before model training, FFANet was used to deblur the images. The effect of FFANet is significant, as shown in Fig. 10 **(a)** and Fig. 10 **(b)**. The images were then labeled by the Labelme software for subsequent analysis.

3.2.2. Evaluation of crack detection models

Similar to the laboratory cases, two DeepLab V3 + models with MobileNet V2 and Xception-65 backbones and the FCN-32 s model with the ResNet101 backbone are trained and compared. The effect of the deblurring process on the crack detection was also checked by applying FFANet before segmentation.

In this section, a total of six models were validated and the semantic segmentation results of these models are shown in Fig. 10. The six models were trained for 1,500 iterations each, which took 40 h per model using our computer. As shown from Fig. 10, the cracks segmented by FFA-DeepLab V3 + models are more complete compared to those without deblurring processing. Among all the models, the FCN-32 s

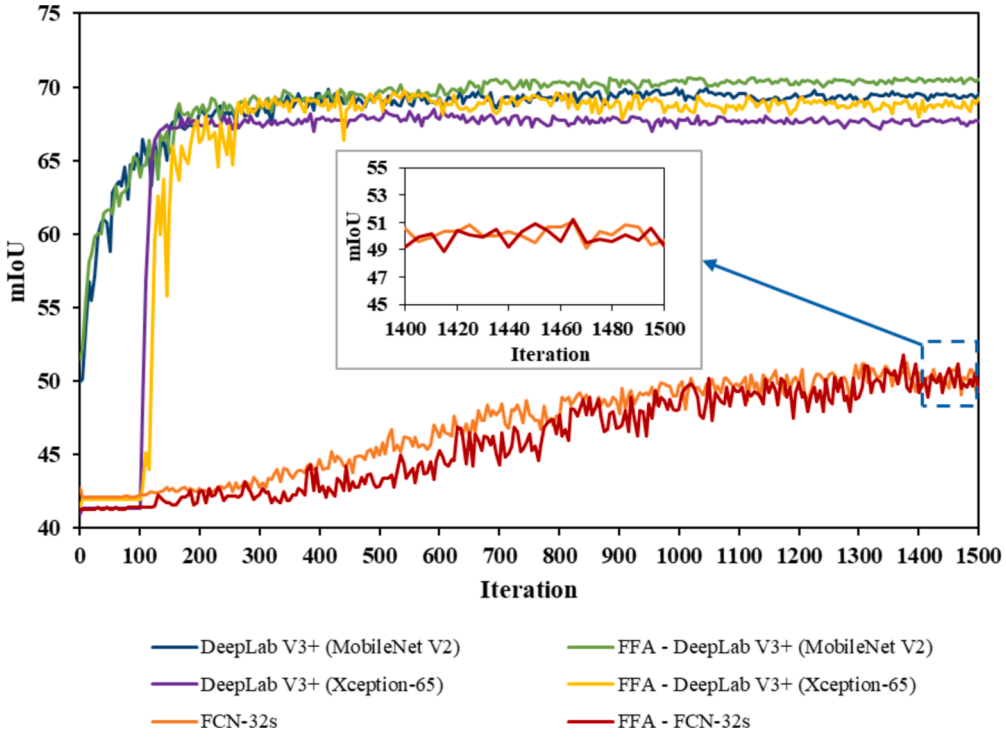

Fig. 11. Variation of mIoU in validation set.

Table 4
Prediction results of different CDC algorithms with actual CCTV images.

Img ID	Image Resolution and Correction factor value	Crack evaluation from field reports	Crack length calculated by CDC with various crack detection models (mm)					
			DeepLab V3+ (MobileNet V2)	DeepLab V3+ (Xception-65)	FCN-32 s	FFA- DeepLab V3+ (MobileNet V2)	FFA- DeepLab V3+ (Xception-65)	FFA-FCN-32 s
1	480 × 260, 2.0	Grade 1, 0–250 mm	302.56	294.68	154.99	357.88	402.83	208.89
2	480 × 260, 2.0	Grade 2, 250–500 mm	267.65	496.76	204.54	319.43	383.55	223.00
3	480 × 260, 2.0	Grade 2, 250–500 mm	551.25	654.25	501.66	611.31	663.59	443.39
4	480 × 260, 2.0	Grade 3, 500–750 mm	655.90	698.68	453.21	617.36	666.22	501.61
5	480 × 260, 2.0	Grade 2, 250–500 mm	127.11	148.82	70.79	132.47	130.71	49.76
6	480 × 260, 2.0	Grade 2, 250–500 mm	427.29	662.87	206.99	423.13	513.66	222.10
7	480 × 260, 2.0	Grade 2, 250–500 mm	610.72	773.27	559.80	846.64	830.85	589.93
8	480 × 260, 2.0	Grade 3, 500–750 mm	811.16	867.37	661.04	783.64	782.94	577.69
9	480 × 260, 2.0	Grade 3, 500–750 mm	850.08	906.77	695.78	753.85	754.89	652.51
10	480 × 260, 2.0	Grade 2, 250–500 mm	325.26	308.68	208.06	335.01	298.87	232.85
11	480 × 260, 2.0	Grade 2, 250–500 mm	316.14	305.33	155.01	273.17	278.50	205.36
12	480 × 260, 2.0	Grade 3, 500–750 mm	272.45	288.01	121.36	298.91	260.30	136.00
13	480 × 260, 2.0	Grade 3, 500–750 mm	890.90	923.65	520.84	694.17	718.53	600.96
14	480 × 260, 2.0	Grade 3, 500–750 mm	354.17	429.76	367.06	412.78	451.24	367.73
15	480 × 260, 2.0	Grade 3, 500–750 mm	485.43	641.98	454.55	712.99	746.93	493.66
16	480 × 260, 2.0	Grade 1, 0–250 mm	259.18	251.80	179.17	241.77	236.70	220.01
17	480 × 260, 2.0	Grade 2, 250–500 mm	328.26	260.82	134.29	433.01	427.57	185.17
18	480 × 260, 2.0	Grade 3, 500–750 mm	614.00	512.24	391.01	563.66	528.01	437.36
19	480 × 260, 2.0	Grade 3, 500–750 mm	688.08	719.41	513.42	617.80	652.47	533.36
20	480 × 260, 2.0	Grade 3, 500–750 mm	721.19	705.61	220.79	679.74	667.31	392.24
21	480 × 260, 2.0	Grade 3, 500–750 mm	805.12	703.99	279.57	706.05	741.48	288.46
22	480 × 260, 2.0	Grade 2, 250–500 mm	375.18	526.51	115.22	381.14	382.62	189.35
23	480 × 260, 2.0	Grade 3, 500–750 mm	566.46	595.21	349.53	738.37	570.36	414.67
24	480 × 260, 2.0	Grade 1, 0–250 mm	123.29	151.26	84.89	144.09	166.02	101.90
25	480 × 260, 2.0	Grade 2, 250–500 mm	547.62	505.68	328.89	598.36	511.93	400.98
26	1920 × 1080, 1.0	Grade 3, 500–750 mm	572.01	570.08	463.76	507.65	545.59	493.42
27	1920 × 1080, 1.0	Grade 2, 250–500 mm	624.25	596.94	490.11	562.83	599.03	496.68
28	1920 × 1080, 1.0	Grade 1, 0–250 mm	151.18	147.31	86.18	132.11	138.61	84.05
29	1920 × 1080, 1.0	Grade 2, 250–500 mm	223.18	208.36	124.92	276.75	301.95	147.83
30	1920 × 1080, 1.0	Grade 3, 500–750 mm	511.19	479.86	441.89	526.37	505.06	404.45
31	1920 × 1080, 1.0	Grade 1, 0–250 mm	297.18	300.97	228.06	322.43	322.55	250.90
32	1920 × 1080, 1.0	Grade 1, 0–250 mm	113.46	125.68	74.21	130.70	134.58	93.57
33	1920 × 1080, 1.0	Grade 2, 250–500 mm	362.26	374.23	242.66	400.22	422.73	289.84
34	1920 × 1080, 1.0	Grade 3, 500–750 mm	452.37	436.48	393.91	525.02	518.51	411.47
35	1920 × 1080, 1.0	Grade 2, 250–500 mm	258.62	234.08	177.89	290.32	288.28	261.33
36	1920 × 1080, 1.0	Grade 3, 500–750 mm	804.41	817.66	799.15	791.28	843.63	784.79
37	1920 × 1080, 1.0	Grade 2, 250–500 mm	418.01	433.69	352.15	445.38	415.85	359.31
38	1920 × 1080, 1.0	Grade 3, 500–750 mm	768.54	772.46	763.58	807.00	815.57	795.95
39	1920 × 1080, 1.0	Grade 3, 500–750 mm	692.10	686.41	541.93	729.50	733.80	606.71
40	1920 × 1080, 1.0	Grade 3, 500–750 mm	580.28	591.90	438.52	526.62	549.30	459.22
41	1920 × 1080, 1.0	Grade 2, 250–500 mm	254.48	265.09	189.86	286.38	251.27	199.99
42	1920 × 1080, 1.0	Grade 3, 500–750 mm	556.66	559.61	487.31	520.43	539.70	494.89
43	1920 × 1080, 1.0	Grade 1, 0–250 mm	301.48	339.78	239.42	244.67	274.16	208.21
44	1920 × 1080, 1.0	Grade 3, 500–750 mm	433.19	435.76	407.87	471.66	455.88	424.37
45	1920 × 1080, 1.0	Grade 2, 250–500 mm	184.73	166.13	50.47	170.47	188.17	62.19
46	1920 × 1080, 1.0	Grade 3, 500–750 mm	581.04	572.11	389.63	530.76	555.23	426.10
47	1920 × 1080, 1.0	Grade 2, 250–500 mm	450.14	427.46	315.17	424.59	393.37	349.17
48	1920 × 1080, 1.0	Grade 1, 0–250 mm	242.96	244.81	214.02	244.80	216.13	218.67
49	1920 × 1080, 1.0	Grade 2, 250–500 mm	314.49	322.96	180.79	337.34	320.49	186.11
50	1920 × 1080, 1.0	Grade 3, 500–750 mm	591.12	600.02	303.40	557.38	575.51	327.53
Accuracy	/	/	**28/50**	**26/50**	**18/50**	**35/50**	**33/50**	**21/50**

*Grades of cracks in the field reports are identified based on *Technical Specification for Inspection and Evaluation of Urban Drainage CJJ 181–2012* (National Development and Reform Commission of the People's Republic of China, 2012).

model has the lowest accuracy, which cannot even detect cracks in some images.

Fig. 11 shows the evaluation of different models based on the mIoU performance metric for the validation dataset. As can be seen from this figure, the DeepLab V3 + models have a higher mIoU accuracy than the FCN-32 s models. This indicates that the DeepLab V3 + algorithm, especially when the backbone is MobileNet V2, has better semantic segmentation performance for sewage pipe cracks than FCN-32 s algorithms. With the deblurring algorithm FFANet, the mIoUs of the two DeepLab V3 + models and FCN-32 s models are improved by 0.7 %, 1.2 % and 0.5 %, respectively, compared to those without FFANet. In all, DeepLab V3 + model with MobileNet V2 backbone and FFANet model has the highest semantic segmentation performance.

3.2.3. Evaluation of crack characterization algorithm

To verify the crack characterization accuracy of the proposed CDC algorithm for the actual CCTV images, 50 images were selected from the validation dataset (35 from Guangzhou and 15 from Hangzhou). The images include various cracks of different morphologies and lengths, and they are accompanied by the field reports provided by the local municipal departments. In this section, the lengths of pipe cracks were calculated by the proposed CDC algorithm based on the actual 1.0-m-diameter pipe. The quality of the CCTV images can cause errors in pipe crack characterization. Therefore, the correction factor α was set to 2.0 for the CCTV images with a resolution of 480 × 266 pixels, and 1.0 for the CCTV images with a resolution of 1920 × 1080 pixels.

The crack characterization results are shown in Table 4. From this

table, the CDC algorithms combined with the DeepLab V3 + models have a better quantification performance than those combined with the FCN-32 s model (which has a quantification accuracy below 50 %). The CDC algorithm with FFANet and DeepLab V3+ (MobileNet V2) performs best by correctly grading 35 out of 50 cracks (i.e., 70 % accuracy), as shown in Table 1. This CDC algorithm also shows the least cases of length prediction deviations over 100 mm (only 5 cases in total) compared to other models. The proposed CDC algorithm performs better than the existing methods the existing methods in Wang et al. (2021) and Jia et al. (2023) (60 % accuracy on average).

In summary, although the calculated crack lengths cannot be directly compared with the real values owing to data limitations, the results of the proposed CDC algorithm are satisfactory with most crack lengths estimated falling within the range specified in the field reports.

4. Conclusions

In this study, we proposed an innovative crack quantification algorithm. Combined with carefully chosen detection model, the new CDC algorithm is proposed to automatically detect and characterize cracks in sewage pipes based on CCTV images for more efficient and accurate pipe defect assessment, contributing to urban water environment management.

The CDC algorithm contains the crack detection model and a newly developed crack characterization algorithm. Its performance was verified using images of pipe cracks created artificially (in the laboratory) and from actual field CCTV inspections. In the laboratory cases, the CDC algorithms with various segmentation models effectively detected and quantified the length of pipe cracks from images. Of these, the CDC algorithm with the DeepLab V3 + segmentation model performed the best. For the filed cases, the CDC algorithm with the DeepLab V3 + segmentation model was also found to be the best-performing algorithm for detecting and characterizing pipe cracks. Additionally, to deal with the blurry images which are commonly seen in real CCTV images, the FFANet deblurring algorithm was introduced. The results showed that the FFANet deblurring algorithm could improve the performance of the CDC algorithms. In summary, the CDC algorithm based on the FFANet and DeepLab V3+ (MobileNet V2) exhibited the best performance. It was considered the optimized model for automated detection and characterization of pipe cracks from CCTV images. Using this method to process the actual CCTV images, 35 out of 50 cracks were correctly graded (i.e., 70 % accuracy), which is better than the existing methods.

The proposed deep-learning-based CDC algorithm was verified on automated quantification of sewage pipe cracks from CCTV images, which can improve the efficiency and accuracy of sewage pipe inspection significantly. Although there are still some uncertainties in calculating longitudinal crack lengths by the proposed method caused by the limitation of CCTV cameras, the deviations are still under control, with a maximum value of less than 30 % in this study. In engineering practice, the CCTV camera can move along the pipe to take photos from different perspectives. The estimation of longitudinal crack lengths by the CDC algorithm can be further reduced using images where most of the cracks were captured near the camera focal plane. In this study, the detection of other pipe defects, like blockage, deformation, etc., is not included. In the future, a more comprehensive algorithm capable of identifying these other pipe defects needs to be developed. Additionally, there is still space for improving the DeepLab V3 + algorithm to improve its accuracy in crack characterization. Also, the correction factor introduced in this study to reduce the effects of image resolution on crack characterization requires further investigation. In future work, we will further optimize the CDC algorithm and the selection principle of correction factors under different image quality conditions.

CRediT authorship contribution statement

Chenhao Yang: Writing – original draft, Methodology, Investigation, Data curation, Conceptualization. **Feifei Zheng:** Writing – review & editing, Supervision, Conceptualization. **Zoran Kapelan:** Writing – review & editing, Supervision, Methodology, Conceptualization. **Dragan Savic:** Writing – review & editing, Supervision, Funding acquisition. **Gang Pan:** Writing – review & editing, Supervision, Methodology. **Yu Feng:** Writing – review & editing, Supervision. **Yiyi Ma:** Writing – review & editing, Supervision, Resources, Methodology, Funding acquisition, Conceptualization.

Declaration of competing interest

The authors declare the following financial interests/personal relationships which may be considered as potential competing interests: [Yiyi Ma reports financial support was provided by National Key R&D Program of China. Yiyi Ma reports financial support was provided by Natural Science Foundation of Zhejiang Province. Yiyi Ma reports financial support was provided by National Natural Science Foundation of China. Dragan Savic reports financial support was provided by European Research Council. If there are other authors, they declare that they have no known competing financial interests or personal relationships that could have appeared to influence the work reported in this paper.].

Acknowledgments

The writers gratefully acknowledge financial support from National Key R&D Program of China (Grant No. 2022YFC3202602), the Natural Science Foundation of Zhejiang Province (Grant No. LZJWZ23E090009), and the National Natural Science Foundation of China (Grant No. 52300122). Dragan Savic has received funding from the European Research Council (ERC) under the European Union's Horizon 2020 research and innovation programme (grant agreement No. [951424]).

Data availability

Data will be made available on request.

References

Altabey, W.A., Noori, M., Wang, T., Ghiasi, R., Kuok, S., Wu, Z., 2021. Deep learning-based crack identification for steel pipelines by extracting features from 3D shadow modeling. Appl. Sci. 11, 6063.

Baah, K., Dubey, B., Harvey, R., Mcbean, E., 2015. A risk-based approach to sanitary sewer pipe asset management. Sci. Total Environ. 505, 1011–1017.

Canny, J., 1986. A computational approach to edge detection. IEEE Trans. Pattern Anal. Mach. Intell. 679–698.

Chen, L., Zhu, Y., Papandreou, G., Schroff, F., Adam, H., 2018. Encoder-Decoder with Atrous Separable Convolution for Semantic Image Segmentation. Computer Vision - ECCV 2018. PT VII 11211, 833–851.

Cheng, J.C.P., Wang, M., 2018. Automated detection of sewer pipe defects in closed-circuit television images using deep learning techniques. Autom. Constr. 95, 155–171.

Diederik P. K and Jimmy B, 2014. Adam: A method for stochastic optimization. [Online]. Available: https://arxiv.org/abs/1412.6980.

Duda, R.O., Hart, P.E., 1972. Use of the Hough transformation to detect lines and curves in pictures. Comm. ACM 11–15.

Everingham, M., Van Gool, L., Williams, C.K.I., Winn, J., Zisserman, A., 2010. The pascal Visual Object Classes (VOC) challenge. Int. J. Comput. vis. 88, 303–338.

Guo, W., Zhang, X., Zhang, D., Chen, Z., Zhou, B., Huang, D., Li, Q., 2022. Detection and classification of pipe defects based on pipe-extended feature pyramid network. Autom. Constr. 141, 104399.

Harpaz, C., Russo, S., Leitao, J.P., Penn, R., 2022. Potential of supervised machine learning algorithms for estimating the impact of water efficient scenarios on solids accumulation in sewers. Water Res. 216, 118247.

Hassan, S.I., Dang, L.M., Mehmood, I., Im, S., Choi, C., Kang, J., Park, Y., Moon, H., 2019. Underground sewer pipe condition assessment based on convolutional neural networks. Autom. Constr. 106, 102849.

Haurum, J.B., Moeslund, T.B., 2020. A survey on image-based automation of CCTV and SSET sewer inspections. Autom. Constr. 111, 103061.

He, K., Zhang, X., Ren, S., Sun, J., 2016. Deep residual learning for image recognition. IEEE Conference on Computer Vision and Pattern Recognition (CVPR) 2016, 770–778.

He, M., Zhao, Q., Gao, H., Zhang, X., Zhao, Q., 2022. Image segmentation of a sewer based on deep learning. Sustainability 14, 6634.
Jia, P., Liao, Y., Zhao, Q., He, M., Guo, M., 2023. Defect severity assessment model for sewer pipeline based on automated pipe calibration. J. Pipel. Syst. Eng. Pract. 14, 1454.
Kumar, S.S., Abraham, D.M., Jahanshahi, M.R., Iseley, T., Starr, J., 2018. Automated defect classification in sewer closed circuit television inspections using deep convolutional neural networks. Autom. Constr. 91, 273–283.
Li, M., Feng, X., Hu, Q., 2023. 3D laser point cloud-based geometric digital twin for condition assessment of large diameter pipelines. Tunn. Undergr. Space Technol. 142. https://doi.org/10.1016/j.tust.2023.105430.
Li, Y., Wang, H., Dang, L.M., Piran, M.J., Moon, H., 2022. A robust instance segmentation framework for underground sewer defect detection. Measurement 190, 110727.
Ma, D., Fang, H., Wang, N., Zheng, H., Dong, J., Hu, H., 2022. Automatic defogging, deblurring, and real-time segmentation system for sewer pipeline defects. Autom. Constr. 144, 104595.
Meijer, D., Scholten, L., Clemens, F., Knobbe, A., 2019. A Defect classification methodology for sewer image sets with Convolutional Neural Networks. Autom. Constr. 104, 281–298.
Moradi, S., Zayed, T., Nasiri, F., Golkhoo, F., 2020. Automated anomaly detection and localization in sewer inspection videos using proportional data modeling and deep learning-based text recognition. J. Infrastruct. Syst. 26, 04020018.
National Development and Reform Commission of the People's Republic of China, 2012. Technical specification for inspection and evaluation of urban drainage CJJ 181 - 2012. Beijing: China Architecture & Building Press.
Oh, C., Dang, L.M., Han, D., Moon, H., 2022. Robust sewer defect detection with text analysis based on deep learning. IEEE Access 10, 46224–46237.
Okwori, E., Viklander, M., Hedstrom, A., 2021. Spatial heterogeneity assessment of factors affecting sewer pipe blockages and predictions. Water Res. 194, 116934.
Pan, G., Zheng, Y., Guo, S., Lv, Y., 2020. Automatic sewer pipe defect semantic segmentation based on improved U-Net. Autom. Constr. 119, 103383.
Qin, X., Wang, Z., Bai, Y., Xie, X., Jia, H., 2020. FFA-Net: Feature Fusion Attention Network for single image dehazing. Thirty-Fourth Aaai Conference on Artificial Intelligence, The Thirty-Second Innovative Applications of Artificial Intelligence Conference and The Tenth Aaai Symposium on Educational Advances in Artificial Intelligence 34, 11908-11915.
Ravanbakhsh, S., Poczos, B., Schneider, J., Schuurmans, D., Greiner, R., 2016. Stochastic neural networks with monotonic activation functions. Artificial Intelligence and Statistics 51 (51), 809–818.
Shi, F., Meng, Q., Pan, L., Wang, J., 2023. Root damage of street trees in urban environments: An overview of its hazards, causes, and prevention and control measures. Sci. Total Environ. 904, 166728.
Sun, L., Zhu, J., Tan, J., Li, X., Li, R., Deng, H., Zhang, X., Liu, B., Zhu, X., 2023. Deep learning-assisted automated sewage pipe defect detection for urban water environment management. Sci. Total Environ. 882, 163562.
Torralba, A., Russell, B.C., Yuen, J., 2010. LabelMe: online image annotation and applications. Proc. Ieee 98, 1467–1484.
Wang, M., Cheng, J., 2019. A unified convolutional neural network integrated with conditional random field for pipe defect segmentation. Comput.-Aided Civil Infrastruct. Eng. 35, 162–177.
Wang, H., Xie, H., Gao, Y., Liujingxu, Song, X., Luo, W., Zhang, Z., Yan, D., 2022. Evaluation method of municipal sewer health status based on YOLOv5. Water Wastewater Eng. 48, 130–136.
Wang, N., Fang, H., Xue, B., Wu, R., Fang, R., Hu, Q., Lv, Y., 2023. Automatic damage segmentation framework for buried sewer pipes based on machine vision: case study of sewer pipes in Zhengzhou, China. J. Infrastruct. Syst. 29, 0000729.
Wang, M., Luo, H., Cheng, J., 2021. Towards an automated condition assessment framework of underground sewer pipes based on closed-circuit television (CCTV) images. Tunn. Undergr. Space Technol. 110, 103840.
Wang, N., Ma, D., Du, X., Li, B., Di, D., Pang, G., Duan, Y., 2024. An automatic defect classification and segmentation method on three-dimensional point clouds for sewer pipes. Tunn. Undergr. Space Technol. 143. https://doi.org/10.1016/j.tust.2023.105480.
Xie, Q., Li, D., Xu, J., Yu, Z., Wang, J., 2019. Automatic detection and classification of sewer defects via hierarchical deep learning. Ieee Trans. Autom. Sci. Eng. 16, 1836–1847.
Xu, Z., Xu, J., Yin, H., Jin, W., Li, H., He, Z., 2019. Urban river pollution control in developing countries. Nat. Sustain. 2, 158–160.
Yin, X., Chen, Y., Bouferguene, A., Zaman, H., Al-Hussein, M., Kurach, L., 2020. A deep learning-based framework for an automated defect detection system for sewer pipes. Autom. Constr. 109, 102967.
Yin, C., Cheng, J.C.P., Wang, B., Gan, V.J.L., 2022. Automated classification of piping components from 3D LiDAR point clouds using SE-PseudoGrid. Autom. Constr. 139, 104300.
Zhao, M., Fang, Z., Ding, N., Li, N., Su, T., Qian, H., 2023. Quantitative detection technology for geometric deformation of pipelines based on LiDAR. Sensors 23. https://doi.org/10.3390/s23249761.